Chaotic dynamics of stellar spin in binaries and the production of misaligned hot Jupiters

Natalia I. Storch *et al.*

Science **345**, 1317 (2014);
DOI: 10.1126/science.1254358

Program, and by the University of California, Lawrence Berkeley National Laboratory under contract no. DE-AC02-05CH11231, Lawrence Livermore National Laboratory under contract no. DE-AC52-07NA27344, and Los Alamos National Laboratory under contract no. DE-AC02-06NA25396. Spectroscopic characterization of RfpA and NpR4776-PCM was funded by a grant from the Chemical Sciences, Geosciences, and Biosciences Division, Office of Basic Energy Sciences, Office of Science, U.S. Department of Energy (DOE DE-FG02-09ER16117 to J.C.L.) The authors thank J. R. Miller for assistance in performing mass analyses on Chls *d* and *f*; B. Stanley and A. Stanley for advice and technical assistance in performing the tryptic peptide mass fingerprinting; and C. Praul and C. Price for assistance in performing RNA-seq profiling. The authors thank J. Lecomte, W. Schluchter, J. Golbeck, and A. Glazer for reading the manuscript and helpful suggestions. This whole-genome shotgun project for *Leptolyngbya* sp. strain JSC-1 (alternative name, *Marsacia ferruginose*; IMG taxon ID 2022827000; GOLD ID = Gi02032) has been deposited at DDBJ/EMBL/GenBank under the accession JMKF00000000; the version described in this paper is version JMKF01000000. RNA-seq data were deposited in the NCBI Sequence Read Archive (SRA) under accession number SRP041154.

SUPPLEMENTARY MATERIALS

www.sciencemag.org/content/full/345/6202/1312/suppl/DC1
Materials and Methods
Figs. S1 to S18
Tables S1 and S2
References (*49–60*)

4 June 2014; accepted 31 July 2014
Published online 21 August 2014;
10.1126/science.1256963

PLANETARY DYNAMICS

Chaotic dynamics of stellar spin in binaries and the production of misaligned hot Jupiters

Natalia I. Storch, Kassandra R. Anderson, Dong Lai*

Many exoplanetary systems containing hot Jupiters are observed to have highly misaligned orbital axes relative to the stellar spin axes. Kozai-Lidov oscillations of orbital eccentricity and inclination induced by a binary companion, in conjunction with tidal dissipation, constitute a major channel for the production of hot Jupiters. We demonstrate that gravitational interaction between the planet and its oblate host star can lead to chaotic evolution of the stellar spin axis during Kozai cycles. As parameters such as the planet mass and stellar rotation period are varied, periodic islands can appear in an ocean of chaos, in a manner reminiscent of other dynamical systems. In the presence of tidal dissipation, the complex spin evolution can leave an imprint on the final spin-orbit misalignment angles.

About 1% of solar-type stars host giant planets with periods of ~3 days (*1*). These "hot Jupiters" could not have formed in situ, given the large stellar tidal gravity and radiation fields close to their host stars. Instead, they are thought to have formed beyond a few astronomical units (AU) and migrated inward. However, the physical mechanisms of the migration remain unclear. In the past few years, high stellar obliquities have been observed in many hot Jupiter systems; that is, the spin axis of the host star and the planetary orbital angular momentum axis are misaligned (*2–7*). Planet migration in protoplanetary disks (*8*, *9*) is usually expected to produce aligned orbital and spin axes [however, see (*10–14*)], so the observed misalignment suggests that other formation channels may be required, such as strong planet-planet scatterings (*15*, *16*), secular interactions or chaos among multiple planets (*17*, *18*), and the Kozai-Lidov effect induced by a distant companion (*19–22*). Other observations suggest that multiple formation channels of hot Jupiters may be required (*23–25*).

In the "Kozai + tide" scenario, a giant planet initially orbits its host star at a few AU and experiences secular gravitational perturbations from a distant companion (a star or planet). When the companion's orbit is sufficiently inclined relative to the planetary orbit, the planet's eccentricity undergoes excursions to large values while the orbital axis precesses with varying inclination. At periastron, tidal dissipation in the planet reduces the orbital energy, leading to inward migration and circularization of the planet's orbit.

As the planet approaches the star in a Kozai cycle, the planet-star interaction torque due to the rotation-induced stellar quadrupole makes the stellar spin axis and the planetary orbital angular momentum axis precess around each other. Although the equations for such precession in the context of triple systems are known (*21*, *26*), previous work on the "Kozai + tide" migration either neglected such spin-orbit coupling or included it without systematically examining the spin dynamics or exploring its consequences for various relevant parameter regimes (*19–22*, *27*). However, the stellar spin has the potential to undergo rich evolution during the Kozai migration, which may leave its traces in the spin-orbit misalignments in hot Jupiter systems. Indeed, there are several examples of chaotic spin-orbit resonances in the solar system. For instance, Saturn's satellite Hyperion experiences chaotic spin evolution due to resonances between spin and orbital precession periods (*28*). The rotation axis of Mars also undergoes chaotic variation as a result of resonances between the spin precession and a combination of orbital precession frequencies (*29*, *30*).

We demonstrate here that gravitational interaction between the stellar spin and the planetary orbit can indeed induce a variety of dynamical behavior for the stellar spin evolution during Kozai cycles, including strongly chaotic behavior (with Lyapunov times as short as a few million years) and perfectly regular behavior in which the stellar spin stays aligned with the orbital axis at all times. We show that in the presence of tidal dissipation, the memory of chaotic spin evolution can be preserved, leaving an imprint on the final spin-orbit misalignment angles.

Center for Space Research, Department of Astronomy, Cornell University, Ithaca, NY 14853, USA.
*Corresponding author. E-mail: dong@astro.cornell.edu

Kozai cycles and spin-orbit coupling

We consider a planet of mass M_p initially in a nearly circular orbit around a star of mass $M_\star$ at a semimajor axis a, with a distant binary companion of mass M_b, semimajor axis a_b, and eccentricity e_b, which we set to 0. In that case, if the planet's initial orbital inclination relative to the binary axis, denoted by θ^0_lb, falls within the range {40°, 140°}, the distant companion induces cyclic variations in planetary orbit inclination and eccentricity, with a maximum eccentricity of $e_\mathrm{max} \approx \sqrt{1-(5/3)\cos^2\theta^0_\mathrm{lb}}$ (*31*, *32*). These Kozai cycles occur at a characteristic rate given by

$$
\begin{aligned}
t_\mathrm{k}^{-1} &= n\left(\frac{M_\mathrm{b}}{M_\star}\right)\left(\frac{a}{a_\mathrm{b}}\right)^3 \\
&= \left(\frac{2\pi}{10^6\ \mathrm{years}}\right)\left(\frac{M_\mathrm{b}}{M_\star}\right)\left(\frac{M_\star}{M_\odot}\right)^{1/2} \\
&\quad\times\left(\frac{a}{1\ \mathrm{AU}}\right)^{3/2}\left(\frac{a_\mathrm{b}}{100\ \mathrm{AU}}\right)^{-3}
\end{aligned}
\quad (1)
$$

where $M_\odot$ is the mass of the Sun and $n = 2\pi/P$ (where P is the orbital period) is the mean motion of the planet. Note, however, that the presence of short-range forces, such as General Relativity and tidal distortions, tends to reduce the maximum attainable eccentricity, so that the actual e_max may be smaller than the "pure" (i.e., without short-range forces) Kozai value given above (*19*, *20*, *33*). Along with the eccentricity and inclination variations, the planetary orbital angular momentum vector precesses around the binary axis ($\hat{\mathbf{L}}_\mathrm{b}$) at a rate that, in the absence of tidal dissipation, is approximately given by

$$
\Omega_\mathrm{pl} \approx \frac{3}{4}t_\mathrm{k}^{-1}\cos\theta^0_\mathrm{lb}\sqrt{1-e_0^2}\left[1-2\left(\frac{1-e_0^2}{1-e^2}\right)\frac{\sin^2\theta^0_\mathrm{lb}}{\sin^2\theta_\mathrm{lb}}\right] \quad (2)
$$

(*34*), where e_0 is the initial eccentricity. Because of the rotation-induced stellar quadrupole, the planet induces precession in the stellar spin orientation, governed by the equation

$$\frac{d\hat{\mathbf{S}}}{dt} = \Omega_{\rm ps}\hat{\mathbf{L}} \times \hat{\mathbf{S}} \qquad (3)$$

where $\hat{\mathbf{S}}$ and $\hat{\mathbf{L}}$ are unit vectors along the stellar spin axis and the planetary orbital angular momentum axis, respectively, and the precession frequency $\Omega_{\rm ps}$ is given by

$$\begin{aligned}\Omega_{\rm ps} &= -\frac{3GM_{\rm p}(I_3 - I_1)}{2a^3(1-e^2)^{3/2}}\frac{\cos\theta_{\rm sl}}{S} \\ &= -2.38\times10^{-8}\left(\frac{2\pi}{\rm years}\right)\frac{1}{(1-e^2)^{3/2}} \\ &\quad\times\left(\frac{2k_{\rm q}}{k_\star}\right)\left(\frac{10^3M_{\rm p}}{M_\star}\right)\left(\frac{M_\star}{M_\odot}\right)^{1/2} \\ &\quad\times\left(\frac{\hat{\Omega}_\star}{0.1}\right)\left(\frac{a}{1\ \rm AU}\right)^{-3}\left(\frac{R_\star}{R_\odot}\right)^{3/2}\cos\theta_{\rm sl} \qquad (4)\end{aligned}$$

where I_3 and I_1 are principal moments of inertia of the star, S is its spin angular momentum, $\hat{\Omega}_\star \equiv \Omega_\star/\sqrt{GM_\star/R_\star^3}$ is its spin frequency in units of the breakup frequency, $R_\star$ is the stellar radius, $R_\odot$ is the radius of the Sun, and $\theta_{\rm sl}$ is the angle between the stellar spin axis and the planet angular momentum axis. We define $(I_3 - I_1) \equiv k_{\rm q}M_\star R_\star^3\hat{\Omega}_\star^2$ and $S \equiv k_\star M_\star R_\star^2\Omega_\star$. For a solar-type star, $k_{\rm q} \approx 0.05$ and $k_\star \approx 0.1$ (35). The stellar quadrupole also affects the planet's orbit by introducing additional periastron advance, at a rate on the order of $-\Omega_{\rm ps}S/(L\cos\theta_{\rm sl})$ (where $L \equiv M_{\rm p}\sqrt{GM_\star a(1-e^2)}$ is the orbital angular momentum), and making $\hat{\mathbf{L}}$ precess around $\hat{\mathbf{S}}$ at the rate $(S/L)\Omega_{\rm ps}$ (34).

During the Kozai cycle, orbital eccentricity varies widely from 0 to $e_{\rm max}$, and thus $\Omega_{\rm ps}$ and $\Omega_{\rm pl}$ change from $\Omega_{\rm ps,0}$ and $\Omega_{\rm pl,0}$ to $\Omega_{\rm ps,max}$ and $\Omega_{\rm pl,max}$, respectively. However, $\Omega_{\rm ps}$ is more sensitive than $\Omega_{\rm pl}$ to eccentricity variation and attains a larger range of values. We therefore expect three qualitatively different regimes for the spin evolution.

Regime I, $|\Omega_{\rm ps,max}| \lesssim |\Omega_{\rm pl,max}|$ ("nonadiabatic"): $|\Omega_{\rm ps}|$ is always smaller than $|\Omega_{\rm pl}|$. We expect $\hat{\mathbf{S}}$ to effectively precess around $\hat{\mathbf{L}}_{\rm b}$, the binary angular momentum axis (about which $\hat{\mathbf{L}}$ is precessing), maintaining an approximately constant angle $\theta_{\rm sb}$.

Regime II, $|\Omega_{\rm ps,max}| \gtrsim |\Omega_{\rm pl,max}|$ and $|\Omega_{\rm ps,0}| \lesssim |\Omega_{\rm pl,0}|$ ("transadiabatic"): A secular resonance occurs when the stellar precession rate approximately matches the orbital precession rate ($|\Omega_{\rm ps}| \approx |\Omega_{\rm pl}|$). As the eccentricity varies from 0 to $e_{\rm max}$ during the Kozai cycle, the system transitions from nonadiabatic to adiabatic. We expect this resonance crossing to lead to complex and potentially chaotic spin evolution.

Regime III, $|\Omega_{\rm ps,0}| \gtrsim |\Omega_{\rm pl,0}|$ ("adiabatic"): $|\Omega_{\rm ps}|$ is always larger than $|\Omega_{\rm pl}|$. We expect the spin axis to follow $\hat{\mathbf{L}}$ adiabatically, maintaining an approximately constant spin-orbit misalignment angle $\theta_{\rm sl}$.

For a given planet semimajor axis a and binary semimajor axis $a_{\rm b}$, the division between different regimes depends on the product of planet mass and stellar spin (fig. S1). In particular, systems with low $M_{\rm p}$ and $\Omega_\star$ lie in regime I, whereas those with large $M_{\rm p}$ and $\Omega_\star$ lie in regimes II and III.

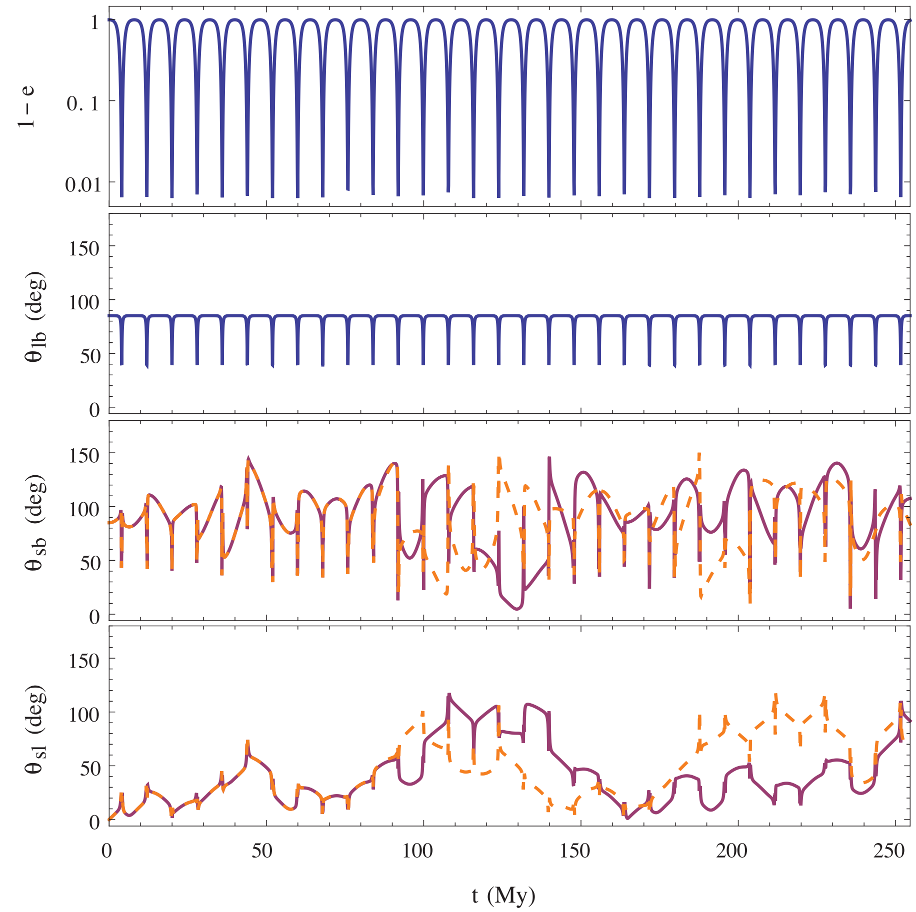

Fig. 1. Sample evolution curves for the "pure" Kozai system, demonstrating how the stellar spin evolves through Kozai cycles. The parameters for this run of 250 million years (My) are a = 1 AU, $a_{\rm b}$ = 200 AU, $e_{\rm b}$ = 0, $M_\star = M_{\rm b} = 1M_\odot$, $\hat{\Omega}_\star$ = 0.05, $M_{\rm p} = 4.6M_J$, and initial e_0 = 0.01, $\theta_{\rm lb}^0$ = 85°. The spin's erratic evolution is suggestive of chaos; we therefore plot a "real" trajectory (red solid lines) and a "shadow" trajectory (orange dashed lines), used to evaluate the degree of chaotic behavior. The trajectories are initialized such that the "real" trajectory starts with $\hat{\mathbf{S}}$ parallel to $\hat{\mathbf{L}}$, whereas the "shadow" trajectory starts with $\hat{\mathbf{S}}$ misaligned by 0.000001° with respect to $\hat{\mathbf{L}}$. This figure corresponds to the orange scatterplot of Fig. 2B and the orange curve of Fig. 3A. The spin evolution is highly chaotic.

Numerical exploration

We first studied the evolution of stellar spin in "pure" Kozai cycles by integrating Eq. 3 together with the evolution equations for the planet's orbital elements, driven by the quadrupole potential from the binary companion (34), but excluding all short-range forces. Although at the octupole level the companion may induce chaotic behavior in the planet orbit (36–39), the effect is negligible if $ae_{\rm b}/[a_{\rm b}(1-e_{\rm b}^2)] \ll 0.01$ and is completely suppressed for $e_{\rm b}$ = 0. To isolate the dynamics of stellar spin evolution, we exclude the precession of $\hat{\mathbf{L}}$ around $\hat{\mathbf{S}}$ and all other short-range forces; thus, although the planet's orbit influences the stellar spin, the stellar spin does not affect the orbit in any way. We consider different combinations of planet mass and stellar rotation rate to illustrate the different regimes described above (we set $M_\star = M_{\rm b} = 1M_\odot$ and $R_\star = 1R_\odot$ in all the examples shown below). We present four "canonical" cases that encapsulate the range of the observed spin dynamics, including a sample trajectory in the transadiabatic regime (regime II) (Fig. 1).

We find excellent agreement with the qualitative arguments outlined above. In the nonadiabatic regime I (Fig. 2A), the spin evolution is regular and periodic. Although we do not plot the spin-binary misalignment angle ($\theta_{\rm sb}$), it indeed stays constant. For trajectories that start with high initial misalignment of $\hat{\mathbf{S}}$ and $\hat{\mathbf{L}}$, the adiabatic regime III (Fig. 2D) is difficult to access because of the $\cos\theta_{\rm sl}$ factor in the spin precession frequency. Those trajectories that start with low initial $\theta_{\rm sl}$ (or with $\theta_{\rm sl}^0$ close to 180°) maintain that angle, as expected. In the transadiabatic regime II, two different types of behavior are observed. For most parameters that fall within this regime, the spin evolution is strongly chaotic, as indicated by the large degree of scatter that fills up the phase space (Fig. 2, B and C). However, periodic islands exist in the middle of this chaos,

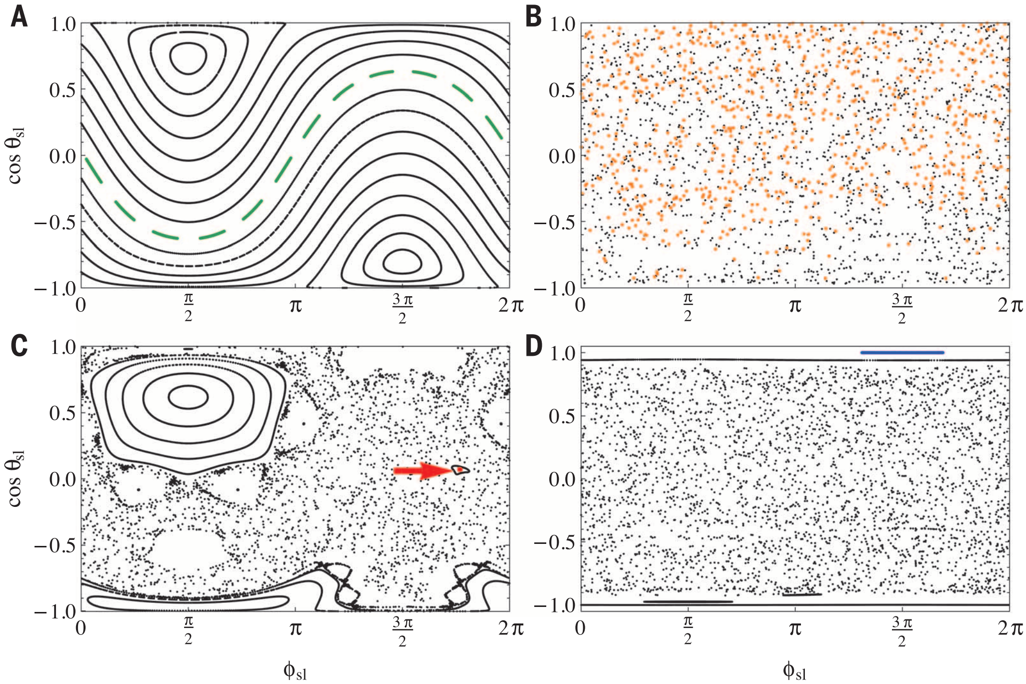

Fig. 2. Surfaces of section of the angle (θ_{sl}) between $\hat{\mathbf{S}}$ and $\hat{\mathbf{L}}$ versus the precessional phase (ϕ_{sl}) of $\hat{\mathbf{S}}$ around $\hat{\mathbf{L}}$ for the "pure" Kozai system, demonstrating the extent of chaos in stellar spin evolution. In all of these sample cases, a = 1 AU, a_b = 200 AU, e_b = 0, $M_\star = M_b = 1M_\odot$, and e_0 = 0.01, θ^0_{lb} = 85°. Each panel is composed of multiple unique trajectories corresponding to different initial values of θ^0_{sl} (with the initial spin-binary angle θ^0_{sb} ranging from 0 to π, and assuming $\hat{\mathbf{S}}$ to be initially in the same plane as $\hat{\mathbf{L}}$ and $\hat{\mathbf{L}}_b$). Each case is evolved for 12.7 billion years, corresponding to ~1500 Kozai cycles. Each point in a trajectory is recorded at the argument of pericenter ω = π/2 (+2πn, with n an integer), corresponding to every other eccentricity maximum (fig. S2). (**A**) Regime I (nonadiabatic); $\hat{\Omega}_\star$ = 0.003, $M_p = 1M_J$. We show 18 unique trajectories, with θ^0_{sb} ranging from 5° to 175°; the green line corresponds to θ^0_{sl} = 0. The "equilibrium" states at (θ_{sl}, ϕ_{sl}) ≈ (40°, 90°) and (40°, 270°) correspond to $\hat{\mathbf{S}}$ parallel and antiparallel to $\hat{\mathbf{L}}_b$. (**B**) Regime II (transadiabatic); $\hat{\Omega}_\star$ = 0.05, $M_p = 4.6M_J$. The orange dots show θ^0_{sl} = 0; the black dots are a composite of several different values of θ^0_{sl}. (**C**) Regime II (transadiabatic); $\hat{\Omega}_\star$ = 0.03, $M_p = 1.025M_J$. There are 11 periodic or quasi-periodic trajectories and a composite chaotic region. An arrow points to the red dot at (cos θ_{sl}, ϕ_{sl}) ≈ (0.06, 1.8π), which corresponds to a periodic island with θ^0_{sl} = 0. (**D**) Regime III (onset of adiabaticity); $\hat{\Omega}_\star$ = 0.05, $M_p = 20M_J$. Five quasi-periodic trajectories and a composite chaotic region are shown. The blue line corresponds to θ^0_{sl} = 0. Note that although both the orange and red cases are found in regime II, the orange one is highly chaotic, and the red resides in a periodic island.

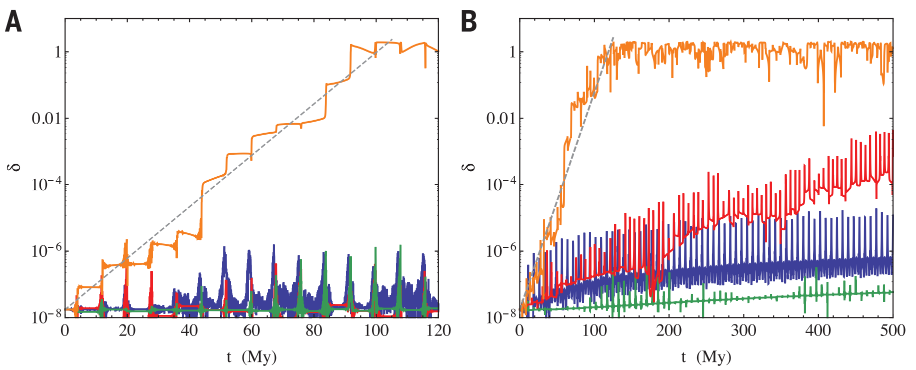

Fig. 3. Distance between two phase-space trajectories starting at slightly different initial spin orientations. (**A**) The "pure" Kozai system. The "real" trajectory starts with $\hat{\mathbf{S}}$ parallel to $\hat{\mathbf{L}}$, and the "shadow" trajectory starts with $\hat{\mathbf{S}}$ misaligned by 0.000001° with respect to $\hat{\mathbf{L}}$, for each of the sample θ^0_{sl} = 0 cases depicted in Fig. 2. The phase-space distance is calculated as $\delta = |\hat{\mathbf{S}}_{real} - \hat{\mathbf{S}}_{shadow}|$ and therefore has a maximum value of 2. The lines are color-coded to correspond to each of the cases of Fig. 2. The gray dashed line demonstrates that for the chaotic orange curve, $\delta \propto e^{\lambda t}$, with λ ≈ 0.18 My^{-1}. (**B**) Same as (A), but including orbit precession due to stellar quadrupole and periastron advances due to General Relativity, stellar quadrupole, planet oblateness, and static tides in the planet. The orange curve shows chaotic growth with λ ≈ 0.15 My^{-1}. The red curve, which is periodic in (A), is mildly chaotic here, with λ ≈ 0.02 My^{-1}.

in which the stellar spin behavior is regular (Fig. 2C and fig. S3).

Because the stellar spin and planet orbital axes in real physical systems typically start out aligned, we focused on the trajectories with $\theta^0_{sl} = 0$. To assess the degree of chaos in each of the sample cases (Fig. 2), we evolved a "shadow" trajectory in addition to the real one (Fig. 1), with initial conditions very close to the original ones, and monitored how quickly the two trajectories diverged, particularly in the spin direction. As expected, three out of our four sample cases did not exhibit chaos; the fourth, in the transadiabatic regime, was strongly chaotic, with a Lyapunov time of λ^{-1} ≈ 5.6 million years, corresponding to only ~1 Kozai cycle (Fig. 3A).

Next, we included the precession of $\hat{\mathbf{L}}$ about $\hat{\mathbf{S}}$ and other short-range forces (periastron advances due to General Relativity, the stellar quadrupole, and the planet's rotational bulge and tidal distortion) (*19*, *20*) in our calculations. We found that including these short-range forces for our four sample cases (Fig. 3B) does not change our general conclusion that chaotic evolution occurs in the transadiabatic regime, although it can shift the locations (in the parameter space) of periodic islands.

Clearly, the stellar spin behavior in the transadiabatic regime is very complex: highly chaotic for certain parameters, more regular for others. To explore this diversity further, we constructed a "bifurcation" diagram (Fig. 4) with which we could examine the degree of chaos over a large range of parameter values (particularly the planet mass). Visualized in this way, the topology of the chaos is more obvious: Most of the mass bins are highly chaotic, but they are interspersed with individual, isolated quasiperiodic islands. To better understand this complex topology, we have developed a simpler analytical toy model that captures many of the features of this system (*34*).

Widespread chaos in dynamical systems is typically driven by overlapping resonances (*40*). Repeated secular spin-orbit resonance crossings ($|\Omega_{ps}| \sim |\Omega_{pl}|$) during Kozai cycles play an important role in producing the observed chaotic spin behavior. On the other hand, Kozai cycles themselves result from the near-1:1 resonance ($\dot{\varpi} = \dot{\Omega}$) between the longitude of the periapse ϖ and the longitude of the ascending node Ω of the planet's orbit. The back-reaction of the stellar spin on the orbit can naturally couple these two resonances. We suggest that all these effects are important in the development of the chaotic stellar spin evolution.

Tidal dissipation and memory of chaotic evolution

Having explored the variety of behaviors exhibited by stellar spin during Kozai cycles, we now assess the impact of this evolution on the production of hot Jupiters, particularly on their final stellar spin-orbit misalignment angles, by adding tidal dissipation to our equations. We used the standard weak friction model of tidal dissipation in giant planets with constant tidal lag time (*41*, *42*). To ensure that all our runs led to circularized planets and a final θ_{sl} within about 10^{10} years, we enhanced tidal dissipation by a factor of 14 (Fig. 5A) and 1400 (Fig. 5B) relative to the fiducial value for Jupiter (*34*, *43*). As long as the tidal evolution time scale of the orbit is much longer than the Lyapunov time for the chaotic spin evolution, we would not expect this enhancement to have a major qualitative effect on the final observed spin-orbit misalignment angle.

We found that tidal dissipation leads to a gradual decrease in the proto–hot Jupiter's semimajor axis and eventual circularization close to the host star (fig. S4). As the planet's orbit decays, Kozai cycles become suppressed by short-range forces. Also, as the semimajor axis decays, $|\Omega_{ps}/\Omega_{pl}|$ increases. Thus, even if we choose initial conditions that lie squarely in the nonadiabatic regime (regime I), as a decreases, all trajectories will eventually go through the $|\Omega_{ps}| = |\Omega_{pl}|$ secular resonance and end up fully adiabatic. At that point, the spin-orbit misalignment angle freezes out to some final, constant value θ_{sl}^{f}.

In all of the numerical examples of nondissipative evolution discussed above, we have held the value of the stellar spin rate $\Omega_\star$ constant. However, because the divisions between different spin evolution regimes depend on $\Omega_\star$, stellar spin-down can potentially have a substantial effect on the degree of chaos in the system. Isolated solar-type stars spin down via magnetic braking associated with the stellar wind (*44*). For simplicity, we use the empirical Skumanich law (*45*) to add stellar spin-down to our evolution equations, starting with an initial spin period of 2.3 days; the final spin period (at t = 5 billion years) is 28 days.

To assess the influence of chaotic stellar spin evolution on the final distribution of spin-orbit misalignment angles, we created a different kind of "bifurcation" diagram (Fig. 5). As in the nondissipative case (Fig. 4), we considered a range of planet masses. For each M_p, we took a set of initial conditions that were identical in all but the initial

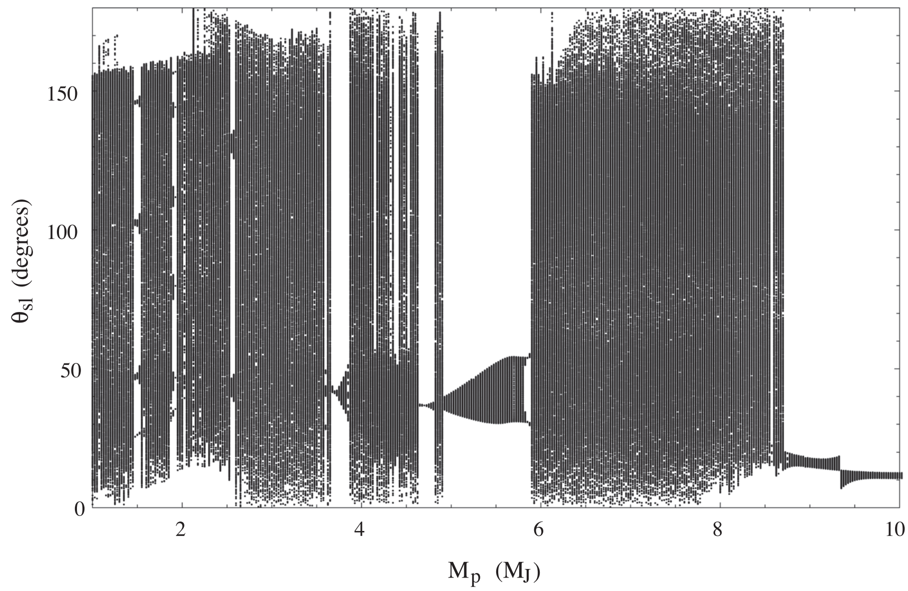

Fig. 4. "Bifurcation" diagram of spin-orbit misalignment angle versus planet mass, including all short-range effects. The procedure described in Fig. 2 is carried out for each value of planet mass; the spin-orbit misalignment angle is recorded at every other eccentricity maximum for ~1500 Kozai cycles. The parameters for this plot are a = 1 AU, a_b = 200 AU, e_0 = 0.01, θ_{lb}^{0} = 85°, $\hat{\Omega}_\star$ = 0.03. A high degree of scatter in a single mass bin indicates highly chaotic behavior. Note that multiple quasi-periodic islands appear in the middle of highly chaotic regions.

Fig. 5. Two "bifurcation" diagrams of the final spin-orbit misalignment angle (top row) and semimajor axis (bottom row) versus planet mass for a small range of initial planet-binary inclinations, including the effects of tidal dissipation and stellar spin-down. Parameters: a_b = 200 AU, e_0 = 0.01, $\hat{\Omega}_{\star,0}$ = 0.05. Each data point represents the outcome of a single complete run, starting with a_0 = 1.5 AU (**A**) and a_0 = 1 AU (**B**) and ending when the planet has sufficiently circularized (final eccentricity $e_f \leq 0.1$) and the final spin-orbit angle θ_{sl}^{f} is attained. For each run, we randomly select an initial inclination θ_{sl}^{0} from the range 86.99° to 87.01° (A) and 84.95° to 85.05° (B). Each mass bin contains ~200 points. The degree of scatter in θ_{sl}^{f} generally increases with increasing M_p but drops sharply in the adiabatic regime [for $M_p \gtrsim 4.4 M_J$ in (A)]. Quasi-periodic islands are still present [e.g., at ~3.8M_J in (B)].

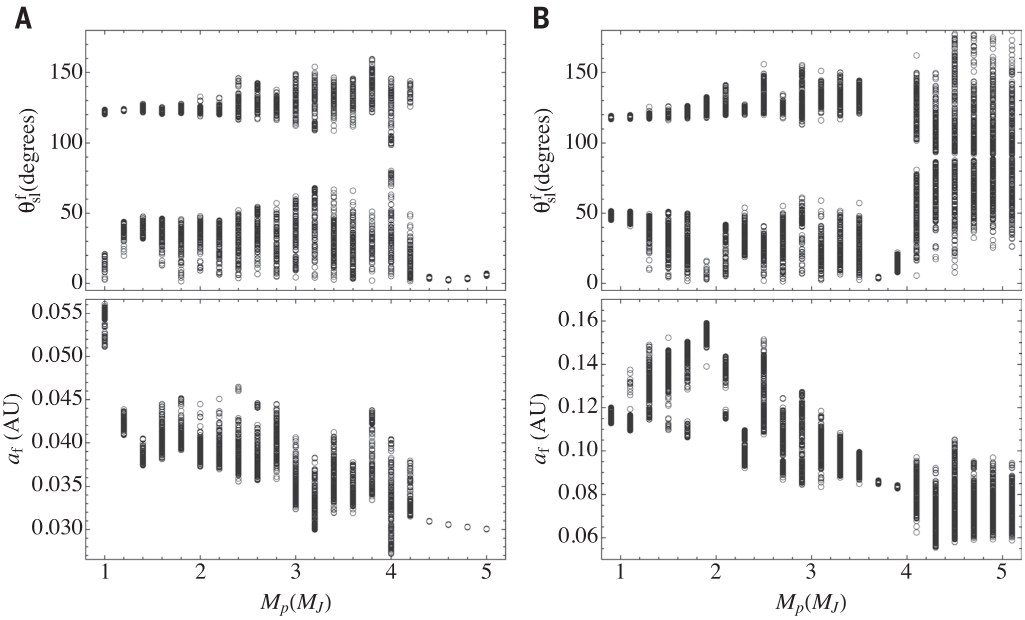

orbit-binary misalignment angle $\theta_{\rm lb}$, which we randomly chose from a very small range: $\theta^0_{\rm lb} \in \{86.99°, 87.01°\}$ (Fig. 5A) and $\theta^0_{\rm lb} \in \{84.95°, 85.05°\}$ (Fig. 5B). We evolved these trajectories until the hot Jupiter circularized and $\theta_{\rm sl}$ reached its final value. We found that the scatter in $\theta^f_{\rm sl}$ depends on the planet mass. The scatter generally increases with increasing $M_{\rm p}$ but drops sharply in the adiabatic regime [for $M_{\rm p} \gtrsim 4.4 M_{\rm J}$ (where $M_{\rm J}$ is the mass of Jupiter) in Fig. 5A]. There also exist quasi-periodic islands where $\theta^f_{\rm sl}$ has a rather small spread. Also, a range of misalignment angles around 90° appears to be excluded, with this range decreasing with increasing planet mass. Given the very small range of initial conditions, the evolution of any regular, nonchaotic system should result in only one final misalignment angle. Therefore, we suggest that this bimodality is the result of the system passing through the $|\Omega_{\rm ps}| \approx |\Omega_{\rm pl}|$ secular resonance and of the complex and possibly chaotic dynamics that occur during that time. We tentatively attribute the decrease of bimodality with increasing mass to an increase in chaotic behavior. The final semimajor axis $a_{\rm f}$ also exhibits "chaotic" spreads and periodic islands. Thus, in effect, the final distributions of $\theta^f_{\rm sl}$ and $a_{\rm f}$ carry an imprint of the spin's past chaotic evolution.

As a final step, we ran a "mini" population synthesis calculation for fixed values of a_0 and $a_{\rm b}$ and a broader range of initial orbital inclinations (Fig. 6). A sharp contrast exists between the distributions of final spin-orbit misalignment

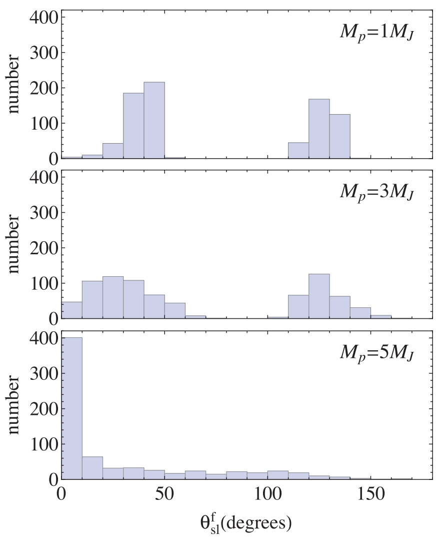

Fig. 6. Distribution of the final spin-orbit misalignment angles as a function of planet mass, including the effects of tidal dissipation and stellar spin-down, for initial planet-binary inclinations $\theta^0_{\rm lb}$ in the range 85° to 89°. Parameters: a_0 = 1.5 AU, $a_{\rm b}$ = 200 AU, e_0 = 0.01, $\hat{\Omega}_{\star,0}$ = 0.05. Each evolutionary trajectory is integrated until it has sufficiently circularized ($e_{\rm f} \leq 0.1$), for a maximum of 5 billion years. If by the end of 5 billion years the planet is not circularized, it is discarded. Note that the bimodality featured in Fig. 5 is still present here, despite the wider range of initial inclinations. At $M_{\rm p} = 5M_{\rm J}$, the evolution is mostly adiabatic, and therefore it is difficult to generate misalignment.

angles at low $M_{\rm p}$ and high $M_{\rm p}$. At low $M_{\rm p}$, a bimodal distribution of $\theta^f_{\rm sl}$ is produced [this bimodality has been found in some previous population synthesis calculations (*20*, *21*)]. At high $M_{\rm p}$, the evolution is mostly adiabatic, producing very little spin-orbit misalignment. This is a clear signature of the complex spin evolution in the observed stellar obliquity. Other factors, such as the stellar spin-down rate and planetary tidal dissipation rate, can also affect the final misalignment distribution.

Discussion

The discovery of spin-orbit misalignment in close-in exoplanetary systems in the past few years was a major surprise in planetary astrophysics. Much of the recent theoretical work has focused on the nontrivial evolution of the planetary orbit (such as orbital flip) due to few-body gravitational interactions (*23*, *37*, *38*). However, as we have shown here, the spin axis of the host star can undergo rather complex and chaotic evolution, depending on the planetary mass and the stellar rotation rate. In many cases, the variation of the stellar spin axis relative to the binary axis is much larger than the variation of the orbital axis. Therefore, to predict the final spin-orbit misalignments of hot Jupiter systems in any high-eccentricity migration scenario, it is important to properly account for the complex behavior of stellar spin evolution.

In the above, we have focused on the Kozai-Lidov mechanism for the formation of hot Jupiters, but similar consideration can be applied to the formation of short-period stellar binaries (*20*). Indeed, spin-orbit misalignment angles have been measured for a number of close-in stellar binaries (*46*–*48*). Because of the much larger stellar spin precession rate in stellar binaries relative to star-planet systems, the stellar spin evolution is expected to be largely in the adiabatic regime (depending on various parameters; fig. S1), in which case the observed spin-orbit misalignment angles in close binaries would reflect their initial values at formation.

It is a curious fact that the stellar spin axis in a wide binary (~100 AU apart) can exhibit such a rich, complex evolution. This is made possible by a tiny planet (~10^{-3} of the stellar mass) that serves as a link between the two stars: The planet is "forced" by the distant companion into a close-in orbit, and it "forces" the spin axis of its host star into wild precession and wandering.

The "binary + planet + spin" system studied here exhibits many intriguing dynamical properties. Although we have provided a qualitative understanding for the emergence of chaos in this system in terms of secular resonance crossing, much remains to be understood theoretically. Most remarkable is the appearance of periodic islands as the system parameters (planet mass and stellar spin) vary—a feature reminiscent of some well-known chaotic systems (*49*, *50*).

REFERENCES AND NOTES

1. S. Udry, N. C. Santos, *Annu. Rev. Astron. Astrophys.* **45**, 397–439 (2007).
2. G. Hébrard *et al.*, *Astron. Astrophys.* **488**, 763–770 (2008).
3. N. Narita, B. Sato, T. Hirano, M. Tamura, *Publ. Astron. Soc. Jpn.* **61**, L35–L40 (2009).
4. J. N. Winn *et al.*, *Astrophys. J.* **703**, L99–L103 (2009).
5. A. Triaud *et al.*, *Astron. Astrophys.* **524**, A25 (2010).
6. G. Hébrard *et al.*, *Astron. Astrophys.* **516**, 95 (2010).
7. S. Albrecht *et al.*, *Astrophys. J.* **757**, 18 (2012).
8. P. Goldreich, S. Tremaine, *Astrophys. J.* **241**, 425 (1980).
9. D. N. C. Lin, P. Bodenheimer, D. C. Richardson, *Nature* **380**, 606–607 (1996).
10. M. R. Bate, G. Lodato, J. E. Pringle, *Mon. Not. R. Astron. Soc.* **401**, 1505–1513 (2010).
11. D. Lai, F. Foucart, D. N. C. Lin, *Mon. Not. R. Astron. Soc.* **412**, 2790–2798 (2011).
12. K. Batygin, *Nature* **491**, 418–420 (2012).
13. K. Batygin, F. C. Adams, *Astrophys. J.* **778**, 169 (2013).
14. D. Lai, *Mon. Not. R. Astron. Soc.* **440**, 3532–3544 (2014).
15. E. B. Ford, F. A. Rasio, *Astrophys. J.* **686**, 621–636 (2008).
16. M. Jurić, S. Tremaine, *Astrophys. J.* **686**, 603–620 (2008).
17. M. Nagasawa, S. Ida, T. Bessho, *Astrophys. J.* **678**, 498–508 (2008).
18. Y. Wu, Y. Lithwick, *Astrophys. J.* **735**, 109 (2011).
19. Y. Wu, N. Murray, *Astrophys. J.* **589**, 605–614 (2003).
20. D. Fabrycky, S. Tremaine, *Astrophys. J.* **669**, 1298–1315 (2007).
21. A. C. M. Correia, J. Laskar, F. Farago, G. Boué, *Celest. Mech. Dynam. Astron.* **111**, 105–130 (2011).
22. S. Naoz, W. M. Farr, F. A. Rasio, *Astrophys. J.* **754**, L36 (2012).
23. R. I. Dawson, R. A. Murray-Clay, *Astrophys. J.* **767**, L24 (2013).
24. S. Dong, B. Katz, A. Socrates, *Astrophys. J.* **781**, L5 (2014).
25. H. Knutson *et al.*, *Astrophys. J.* **785**, 126 (2014).
26. P. P. Eggleton, L. Kiseleva-Eggleton, *Astrophys. J.* **562**, 1012–1030 (2001).
27. Y. Lithwick, Y. Wu, *Proc. Natl. Acad. Sci. U.S.A.* 10.1073/pnas.1308261110 (2014).
28. J. Wisdom, S. J. Peale, F. Mignard, *Icarus* **58**, 137–152 (1984).
29. J. Laskar, P. Robutel, *Nature* **361**, 608–612 (1993).
30. J. Touma, J. Wisdom, *Science* **259**, 1294–1297 (1993).
31. Y. Kozai, *Astron. J.* **67**, 591 (1962).
32. M. L. Lidov, *Planet. Space Sci.* **9**, 719–759 (1962).
33. M. Holman, J. Touma, S. Tremaine, *Nature* **386**, 254–256 (1997).
34. See supplementary materials on *Science* Online.
35. A. Claret, A. Gimenez, *Astron. Astrophys. Suppl. Ser.* **96**, 255 (1992).
36. E. B. Ford, B. Kozinsky, F. A. Rasio, *Astrophys. J.* **535**, 385–401 (2000).
37. B. Katz, S. Dong, R. Malhotra, *Phys. Rev. Lett.* **107**, 181101 (2011).
38. S. Naoz, W. M. Farr, Y. Lithwick, F. A. Rasio, J. Teyssandier, *Nature* **473**, 187–189 (2011).
39. S. Naoz, W. M. Farr, Y. Lithwick, F. A. Rasio, J. Teyssandier, *Mon. Not. R. Astron. Soc.* **431**, 2155–2171 (2013).
40. B. V. Chirikov, *Phys. Rep.* **52**, 263–379 (1979).
41. M. E. Alexander, *Astrophys. Space Sci.* **23**, 459–510 (1973).
42. P. Hut, *Astron. Astrophys.* **99**, 126–140 (1981).
43. N. I. Storch, D. Lai, *Mon. Not. R. Astron. Soc.* **438**, 1526–1534 (2014).
44. F. Gallet, J. Bouvier, *Astron. Astrophys.* **556**, A36 (2013).
45. A. Skumanich, *Astrophys. J.* **171**, 565 (1972).
46. S. Albrecht, S. Reffert, I. A. Snellen, J. N. Winn, *Nature* **461**, 373–376 (2009).
47. A. H. M. J. Triaud *et al.*, *Astron. Astrophys.* **549**, A18 (2013).
48. S. Albrecht *et al.*, *Astrophys. J.* **785**, 83 (2014).
49. S. H. Strogatz, *Nonlinear Dynamics and Chaos: With Applications to Physics, Biology, Chemistry, and Engineering* (Perseus, Reading, MA, 1994).
50. A. J. Lichtenberg, M. A. Lieberman, *Regular and Chaotic Dynamics* (Springer, New York, 1992).

ACKNOWLEDGMENTS

We thank K. Batygin, D. Fabrycky, M. Holman, and D. Muñoz for useful discussions. Supported by NSF Graduate Research Fellowship Program grant DGE-1144153 (K.R.A.), NSF grants AST-1008245 and AST-1211061, and NASA grants NNX12AF85G and NNX14AG94G.

SUPPLEMENTARY MATERIALS

www.sciencemag.org/content/345/6202/1317/suppl/DC1
Materials and Methods
Supplementary Text
Figs. S1 to S7

3 April 2014; accepted 30 July 2014
10.1126/science.1254358